Geophysical Research Letters

RESEARCH LETTER
10.1029/2018GL078498

Ion-Scale Kinetic Alfvén Turbulence: MMS Measurements of the Alfvén Ratio in the Magnetosheath

O. W. Roberts[1], S. Toledo-Redondo[2], D. Perrone[3], J. Zhao[4], Y. Narita[5], D. Gershman[6], R. Nakamura[5], B. Lavraud[7], C. P. Escoubet[1], B. Giles[6], J. Dorelli[6], C. Pollock[6], and J. Burch[8]

[1]ESA-ESTEC, European Space Agency, Noordwijk, Netherlands, [2]ESA-ESAC, European Space Agency, Madrid, Spain, [3]Department of Physics, Imperial College London, London, UK, [4]Key Laboratory of Planetary Sciences, Purple Mountain Observatory, Chinese Academy of Sciences, Nanjing, China, [5]Space Research Institute, Austrian Academy of Sciences, Graz, Austria, [6]NASA Goddard Space Flight Center, Greenbelt, MD, USA, [7]Institut de Recherche en Astrophysique et Planétologie, CNRS, UPS, CNES, Université de Toulouse, Toulouse, France, [8]Southwest Research Institute, San Antonio, TX, USA

Key Points:
- The Alfvén ratio is measured for the first time at ion kinetic scales in the magnetosheath
- The Alfvén ratio shows the better agreement with the prediction for kinetic Alfvén rather than kinetic slow turbulence
- Normalized ratio of the trace magnetic and electron density fluctuations rule out magnetosonic turbulence as the dominant process

Correspondence to:
O. W. Roberts,
o.wyn.roberts@gmail.com

Citation:
Roberts, O. W., Toledo-Redondo, S., Perrone, D., Zhao, J., Narita, Y., Gershman, D., et al. (2018). Ion-scale kinetic Alfvén turbulence: MMS measurements of the Alfvén ratio in the magnetosheath. *Geophysical Research Letters*, *45*, 7974–7984. https://doi.org/10.1029/2018GL078498

Received 24 APR 2018
Accepted 5 JUL 2018
Accepted article online 11 JUL 2018
Published online 21 AUG 2018

Abstract Turbulence in the Earth's magnetosheath at ion kinetic scales is investigated with the magnetospheric multiscale spacecraft. Several possibilities in the wave paradigm have been invoked to explain plasma turbulence at ion kinetic scales such as kinetic Alfvén, slow, or magnetosonic waves. To differentiate between these different plasma waves is a challenging task, especially since some waves, in particular, kinetic slow waves and kinetic Alfvén waves, share some properties making the possibility to distinguishing between them very difficult. Using the excellent time resolution data set provided from both the fluxgate magnetometer and the Fast Plasma Instrument, the ratio of trace velocity fluctuations to the magnetic fluctuations (in Alfvén units), which is termed the Alfvén ratio, can be calculated down to ion kinetic scales. Comparison of the measured Alfvén ratio is performed with respect to the expectation from two-fluid magnetohydrodynamic theory for the kinetic slow wave and kinetic Alfvén wave. Moreover, the plasma data also allow normalized fluctuation amplitudes of density and magnetic field to be compared differentiating between magnetosonic-like and kinetic Alfvén-like turbulence. Using these two different ratios, we can rule out that the fluctuations at ion scales are dominated by magnetosonic-like fluctuations or kinetic slow-like fluctuations and show that they are consistent with kinetic Alfvén-like fluctuations. This suggests that in the wave paradigm, heating in the direction of the parallel magnetic field is predominantly by the Landau damping of the kinetic Alfvén wave.

Plain Language Summary In this study, we have sought to characterize the nature of magnetic fluctuations in the Earth's magnetosheath by using a combination of velocity, density, and magnetic field measurements. We are able to determine that the fluctuations are dominated by kinetic Alfvén wave (KAW) fluctuations at these scales rather than kinetic slow or magnetosonic fluctuations. There have been several previous studies that have highlighted the importance of the KAW; however, theoretically, the wave shares a number of properties with the kinetic slow wave. One property that differs significantly is the Alfvén ratio (the ratio of velocity to magnetic fluctuations) where velocity fluctuations dominate for the kinetic slow wave and magnetic fluctuations dominate for the KAW. With the exceptional time resolution of both plasma and magnetic field data from NASA's Magnetospheric Multiscale mission, this ratio can be measured for the first time down to proton scales. The dominance of the KAW or KAW-like fluctuations is confirmed from the ratio since it decreases significantly at lengths close to that of the proton characteristic scales.

1. Introduction

Turbulence is a phenomenon that is characterized by disordered fluctuations over a large range of scales (Bruno & Carbone, 2013; Kiyani et al., 2015). These fluctuations are observed in the electromagnetic fields (Alexandrova et al., 2012, 2013; Bale et al., 2005; Kiyani et al., 2015; O. W. Roberts, Narita & Escoubet, 2017), as well as in density (Celnikier et al., 1983; Chen, Salem, et al., 2012; O. W. Roberts et al., 2018a, 2018b; O. W. Roberts, Narita, Li, et al., 2017), velocity, and temperature (Podesta, 2006; Šafránková et al., 2013, 2016). However, sampling frequencies of plasma fluctuations are low (as compared to magnetic field fluctuations) making it often difficult to compare different parameters directly.

Studies of plasma turbulence have been mainly focused on the solar wind. However, the Earth's magnetosheath also provides an easily accessible laboratory where turbulence can be investigated, although some differences have to be taken into account (e.g., Alexandrova et al., 2008). In the magnetosheath, different wave modes and nonlinear coherent structures, not commonly associated with the solar wind, are often observed (see the review of Lucek et al., 2005). Typically, the plasma is more compressed, hotter, and denser and has lower bulk speed than in the solar wind, and often, ion temperature, T_i, is higher than electron temperature, T_e ($T_i > T_e$). Additionally, in the magnetosheath, the ion temperature in the direction perpendicular to the magnetic field is often larger than the temperature in the parallel direction ($T_{i\perp} > T_{i\parallel}$). This is favorable to the development of the ion cyclotron instability at $\beta \lesssim 1$ (Alexandrova et al., 2004) or of the mirror instability at $\beta \gtrsim 3$ (Génot et al., 2009), with β being the ratio between the plasma thermal pressure and the magnetic pressure, whereas in the solar wind, the temperatures tend to be more isotropic ($T_{p\parallel} \gtrsim T_{p\perp}$; Hellinger et al., 2006).

Recently, kinetic Alfvén waves (KAWs) have been invoked to explain the morphology of the spectrum at ion kinetic scales in the solar wind (e.g., He et al., 2012; Podesta, 2013; Sahraoui et al., 2010; Salem et al., 2012; Telloni et al., 2015) and in the magnetosheath (Chen & Boldyrev, 2017). Multispacecraft observations of solar wind plasma at ion scales often reveal slowly propagating fluctuations in the plasma frame with low intrinsic frequencies $\omega_{\text{pla}} \sim 0$ (e.g., Perrone et al., 2017; O. W. Roberts et al., 2013, 2015). This result has been interpreted either as KAW turbulence (Sahraoui et al., 2010), coherent structures which are mostly advected in by the bulk flow (Perrone et al., 2016, 2017; O. W. Roberts et al., 2016), a mixture of KAWs and advected structures (Perschke et al., 2016; O. W. Roberts et al., 2013, 2015), or nonlinear fluctuations (Perschke et al., 2014; O. W. Roberts, Narita, Li, et al., 2017). Until recently, the role of kinetic slow waves (KSWs) have largely been ignored as it is heavily damped for the typical plasma parameters of the solar wind (Barnes, 1966; Narita & Marsch, 2015). Recently, KSWs (or pressure balanced structures) have often been invoked to explain the compressible fluctuations and the anticorrelation of magnetic field strength, B, and the density, n, at fluid scales (Howes et al., 2012; Verscharen et al., 2017) and have also been revisited at sub-ion scales to explain the observed increase in compressibility (Lacombe et al., 2017). An alternative explanation is that the increased compressibility may be due to KAWs which become more compressible as they reach smaller scales (e.g., Kiyani et al., 2013). Furthermore, the compressibility of the KAWs may be enhanced even further when effects related to the electron inertial scale become important (Chen & Boldyrev, 2017; Passot et al., 2017).

Determining which wavemodes are dominant in the plasma allows a better understanding of the compressibility in the plasma, as well as the energy budget for particle heating. Different wavemodes exchange energy with particles by different mechanisms including (i) cyclotron resonance which heats in the direction perpendicular to the magnetic field and broadens the velocity distribution function in the perpendicular direction; (ii) Landau resonance which heats in the direction parallel to the magnetic field and can give a parallel beam in the velocity distribution function (VDF); and (iii) pitch angle scattering which can lead to the formation of a plateau in the VDF (e.g., Tu et al., 2002). Both KAWs and KSWs damp by Landau resonance with protons; however, as the damping rate of KAWs are smaller, energy may be available at smaller scales to heat electrons (Howes et al., 2011). However, as the KSW is left-hand polarized (as opposed to the KAW), it can interact with protons by pitch angle scattering which might play a role for the shaping the VDF and, in some cases, can lead to proton heating in the perpendicular direction (Narita & Marsch, 2015).

Differentiating between KAW and KSW is a challenging task as both waves share many properties such as an anticorrelation of magnetic field B and density n, and their theoretical dispersion relation is similar (e.g., Narita & Marsch, 2015). Moreover, several studies of the dispersion relation in the solar wind have demonstrated that the obtained points on the dispersion relation diagram are scattered, and a single plasma wave as predicted from Vlasov theory cannot be found (Narita & Motschmann, 2017; Narita, 2018; O. W. Roberts et al., 2015). The scatter seen in these diagrams has been interpreted as being due to the presence of wave-wave interactions (Howes, 2013; Narita & Motschmann, 2017; O. W. Roberts, Narita, Li, et al., 2017). Furthermore, the error on the velocity measurement used in the Doppler shift calculation is significant making interpretation more difficult.

To definitively identify whether KAWs or KSWs are the dominant wave-like fluctuations, Zhao et al. (2014) proposed three measurements. The first two are polarization and magnetic helicity, where polarization refers to the temporal rotation sense of the magnetic field vector about the mean magnetic field, while helicity refers to the spatial sense of rotation of the magnetic field vector. It should be noted that if single spacecraft is used,

we can only measure the reduced magnetic helicity (Matthaeus & Goldstein, 1982). Essentially, we can only measure the helicity along a single path through the plasma.

Converting from a time series sampled by a single spacecraft to a spatial series through the plasma is not trivial but can be done under certain conditions. To Doppler shift from the spacecraft frame (subscript sc) into the plasma frame (subscript pla), equation (1) can be used.

$$\omega_{sc} = \omega_{pla} + \mathbf{k} \cdot \mathbf{V_i}. \tag{1}$$

Here ω is the angular frequency in both frames of reference, $\mathbf{k}$ denotes the wavevector, and $\mathbf{V_i}$ denotes the bulk velocity (ion velocity in our case). However, $\mathbf{k}$ and ω_{pla} are often both unknowns. This can be overcome when the evolution of the fluctuations is slower than the time taken to pass over the spacecraft (i.e., when $\mathbf{k}\cdot\mathbf{V_i} \gg \omega_{pla}$ such that $\omega_{sc} \simeq \mathbf{k}\cdot\mathbf{V_i}$), and the corresponding relation between linear frequency in the spacecraft frame and wavenumber $f_{sc} = \mathbf{k}\cdot\mathbf{V_i}/2\pi$ can be used. When the condition for this hypothesis is true, the helicity and polaraization are related, that is, positive helicity being related to right-hand polarization. However, the helicity measurement assumes that the direction of propagation is known and is often assumed to be along the bulk flow direction. Thus, these measurements can be ambiguous (Narita & Glassmeier, 2009; O. W. Roberts et al., 2018a) and require a simultaneous measurement of direction of propagation for the fluctuations to be certain of the sense of polarization. Additionally, coherent structures which are not wave-like in nature can give a polarization signature similar to a plasma wave (Perrone et al., 2017).

The final property suggested by Zhao et al. (2014) is the Alfvén ratio, which is the ratio of the trace velocity fluctuations to the trace magnetic fluctuations in Alfvén units which is defined in equation 2.

$$R_A = \mu_0 n m_i \frac{|\delta \mathbf{V}_i|^2}{|\delta \mathbf{B}|^2}. \tag{2}$$

Several studies of the Alfvén ratio have been performed previously in the solar wind at magnetohydrodynamic (MHD) scales, since the time resolution of velocity measurements is typically too low to probe ion kinetic scales. These have revealed that in Alfvénic intervals of solar wind at MHD scales in the inner heliosphere (i.e., at heliocentric distances smaller than 1 AU), the Alfvén ratio is larger than 1 (D. A. Roberts et al., 1990), whereas at a heliocentric distance of 1 AU, the ratio is smaller than unity (Bruno et al., 1985; Matthaeus & Goldstein, 1982; Tu et al., 1989) and decreases further as the heliocentric distance increases (D. A. Roberts et al., 1990). It should be noted that in non-Alfvénic winds, the radial evolution is less marked, and magnetic energy has been shown to dominate at all distances measured in the inner heliosphere (Bruno et al., 2007; Bruno & Carbone, 2013). Furthermore, the ratio may be reduced by discontinuities in the magnetic field (Borovsky, 2008) and may be increased when the presence of alpha particles, heavier ions, and pressure anisotropies are accounted for (Chen, Bale, et al., 2013). At MHD scales, the Alfvén ratio is expected to be similar for both KAWs and KSWs and is sensitive to the value of plasma β (Zhao et al., 2014). At ion kinetic scales, the predicted Alfvén ratio from the two fluid approach in Zhao et al. (2014), diverges from unity with $R_{A,\mathrm{KAW}} \ll 1$ and $R_{A,\mathrm{KSW}} \gg 1$. Moreover, using linear Vlasov theory for $\beta \sim 1$ and $T_i = T_e$, Gary (1986) showed that Alfvén ratio of quasi-perpendicular KAWs also decreases from unity with increasing wavenumber, while quasi-perpendicular magnetosonic waves have a ratio larger than $R_{A,MS} > 2$.

The goal of this study is to use the exceptional time resolution of the Fast Plasma Instrument (FPI; Pollock et al., 2016), in tandem with the magnetic field measurements from the digital fluxgate magnetometer (Russell et al., 2016) on board the Magnetospheric Multiscale (MMS) spacecraft (Burch et al., 2016) to obtain, for the first time, the Alfvén ratio at ion kinetic scales. The evolution of the Alfvén ratio as a function of spacecraft frequency can then be used as a marker to identify whether fluctuations at ion kinetic scales are dominated by kinetic Alfvén-like fluctuations or kinetic slow-like fluctuations. Moreover, we can simultaneously investigate the ratio of normalized electron density and trace magnetic field fluctuations to determine whether the turbulence is KAW-like or magnetosonic-like (Chen, Boldyrev, et al., 2013).

2. Data

MMS was launched in 2015 and inserted into an Earth's equatorial orbit (Burch et al., 2016). It is composed of four identical spacecraft flying in tetrahedron with spacecraft separations that range from about 4 km to a few tens of kilometers. Each spacecraft carries a suite of instruments that allow sampling the fields and the

particles with unprecedented detail. We use burst mode data from MMS1 when it was in the subsolar magnetosheath region, between 13:57:54 and 14:04:24 on 10 November 2015. The interval was selected such that it could be long enough to resolve the inertial range but short enough so that the plasma parameters in the interval vary as little as possible. The measured data from MMS1 are given in Figure 1. The measurements are provided using Geocentric Solar Ecliptic coordinates where the x coordinate points from Earth to the Sun and z points to the ecliptic north direction. In particular, panel (a) shows the magnetic field components and magnitude; panel (b) the ion and electron densities; panel (c) the ion velocity components and magnitude; panel (d) the omnidirectional ion spectrogram plus the ion parallel and perpendicular temperatures; and panel (e) the omnidirectional electron spectrogram plus the electron parallel and perpendicular temperatures. The magnetic field is sampled at a frequency of 128 Hz, while the ion and electron data are sampled at 6.6 and 33.3 Hz, respectively. During the interval of Figure 1, the average plasma β parameter is 0.98 ± 0.49, and the average ion density and bulk speeds are $n_i = 8.3 \pm 1.4$ cm^{-3} and $V_i = 209 \pm 49$ km/s, respectively. Finally, the mean ratio of electron to ion temperatures is $T_e/T_i = 0.084 \pm 0.016$. It is important to note that FPI-Dual Ion Spectrometer measures ions and does not discriminate between species; however, the magnetosheath is dominated by protons, and we expect contributions from alphas and heavier nuclei to be small.

The trace wavelet (Torrence & Compo, 1998) spectrum of the Alfvén velocity is given in Figure 2a, where the magnetic field is resampled to the FPI ion sampling frequency and then normalized into Alfvén units using the ion density measurement. If the data are normalized to the electron density data, we obtain similar spectra; the electron velocity spectra reach the noise floor before the ion velocity measurement; therefore, we will use the ion velocity and density. Figures 2b–2d show the trace ion velocity, ion density, and electron density wavelet power spectra, respectively. The solid gray curve denotes the estimation of the instrument noise floor for the interval following the method described by Gershman et al. (2018). The dashed gray line gives the noise floor estimate multiplied by 3 (note that no gray line is shown in panel (a) since the noise level is several orders of magnitude below the signal). The blue vertical dashed line indicates the maximum frequency (f_{max}) where the signal is more than 3 times the noise level. Above this frequency, the spectrum is influenced significantly by the instrumental noise (e.g., Alexandrova et al., 2010, 2012; O. W. Roberts, Alexandrova, et al., 2017). The green dot-dashed and purple solid lines denote the Taylor shifted ion inertial length $f_{\lambda i} = V_i/2\pi\lambda_i$ and gyroradius $f_{\rho i} = V_i/2\pi\rho_i$, respectively; however, they are very close to one another as $\beta \sim 1$.

The orange dashed lines denote the spectral indices obtained for the spectra fitted in the frequency range [0.08–0.4] Hz for the low-frequency (inertial) scales of all spectra. The lower frequency bound is chosen to avoid cone of influence effects, while the upper bound was selected to avoid the start of the ion kinetic range near $f_{\rho i} \sim f_{di} \sim 0.5$ Hz. For the high frequency (ion kinetic) range, the spectra are fitted for different ranges due to differences in the location of the noise floor for each measurement. For spectra (a) and (b), the fitting is performed between [0.6–f_{Max}]. However, for density spectra in (c) and (d), a transition (flattening) is observed for a small range of scales before the spectrum steepens further motivating a larger lower bound for the fitting of 0.95 Hz. Meanwhile, the maximum physical frequency is 1.6 Hz for the ion density in (c) and 4.5 Hz for the electron density in (d).

The transition range in the density spectra has been shown to be sensitive to the value of plasma β (e.g., Chen, Howes, et al., 2012) with smaller values of β being associated with a transition range that extends over a larger range of frequencies. This has been interpreted as a result of two processes at large and small scales and the crossover point where one process begins to dominate the other depends on β. At large scales, the compressible component cascades passively with respect to the incompressible component (Alfvén waves and slow waves cascade but do not interact). At kinetic scales, the Alfvén wave transitions to the KAW and becomes more compressible, and then KSWs and KAWs can now interact (Chandran et al., 2009, Chen, Howes, et al., 2012,Schekochihin et al., 2009).

The results for the V_A spectrum are consistent with those often found in the solar wind for the magnetic field, being close to the Kolmogorov −5/3 power law at inertial scales before steepening after the spectral break (e.g., Bruno et al., 2014; Smith et al., 2006). Meanwhile, velocity spectrum is flatter at inertial scales before steepening more prominently after the spectral break again similarly to the solar wind case (Šafránková et al., 2013, 2016).

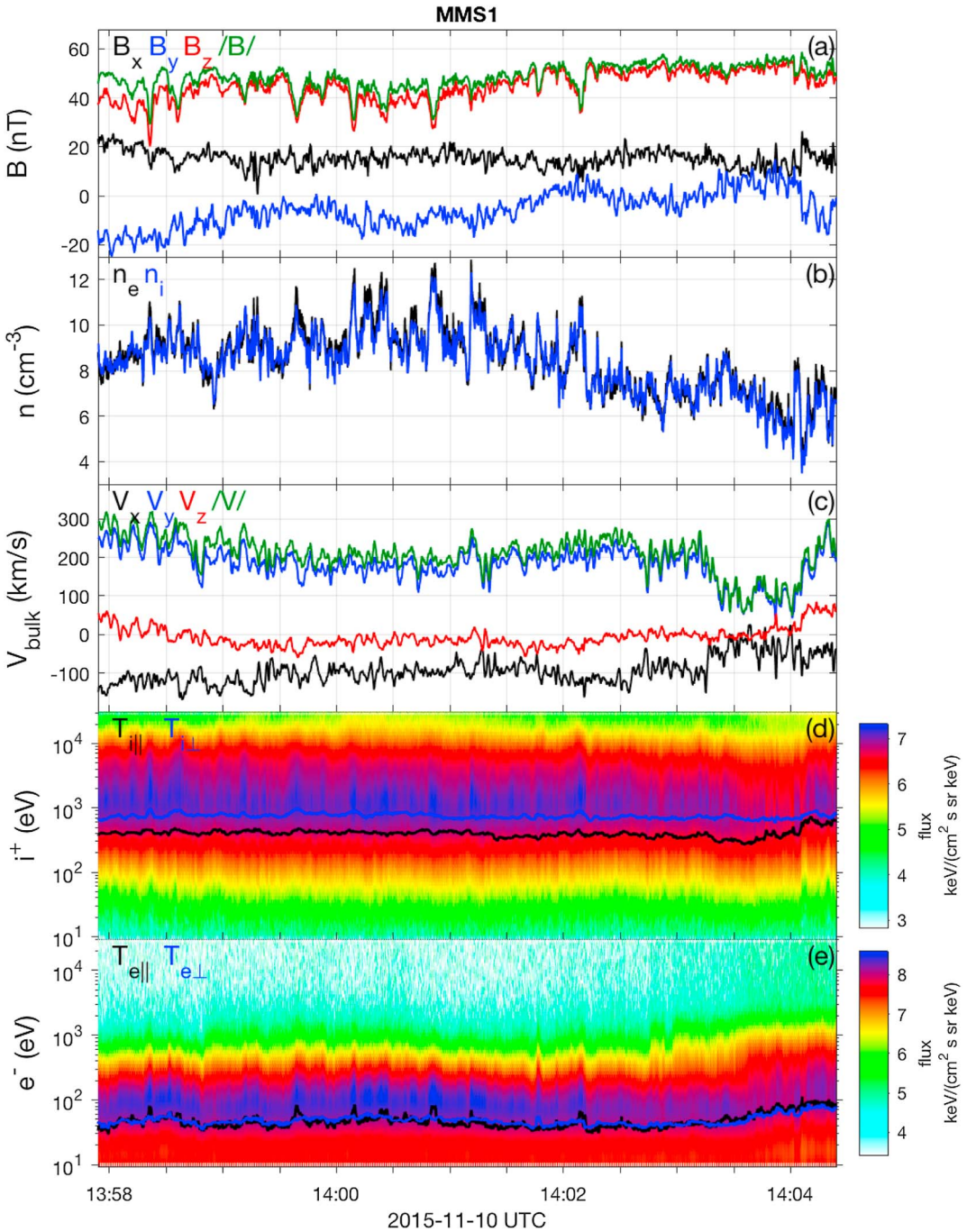

Figure 1. Measured data from Magnetospheric Multiscale 1 (MMS1) in the interval 13:57:54–14:04:24 on the November 2015 in Geocentric Solar Ecliptic coordinates. (a) Magnetic field components and magnitude, (b) ion and electron number densities, (c) ion bulk velocities, and (d) ion differential energy flux spectrogram. Parallel (black) and perpendicular (blue) temperatures are plotted on top. (e) Electron differential energy flux spectrogram. Parallel (black) and perpendicular (blue) temperatures are plotted on top. UTC = universal time coordinated.

3. Results

Figure 3a shows the observed Alfvén ratio obtained from the spectra presented in Figures 2a and 2b. The rose-colored area shows the relative error, defined as $\sigma_{R_A,\mathrm{rel}} = \frac{\sigma_{R_A}}{R_A \ln 10}$ where σ_{R_A} is the standard deviation of the Alfvén ratio. This is calculated based on the propagation of the standard deviations of the trace Alfvén velocity and the trace ion velocity spectra. The ratio R_A is plotted as a function of the frequency measured in

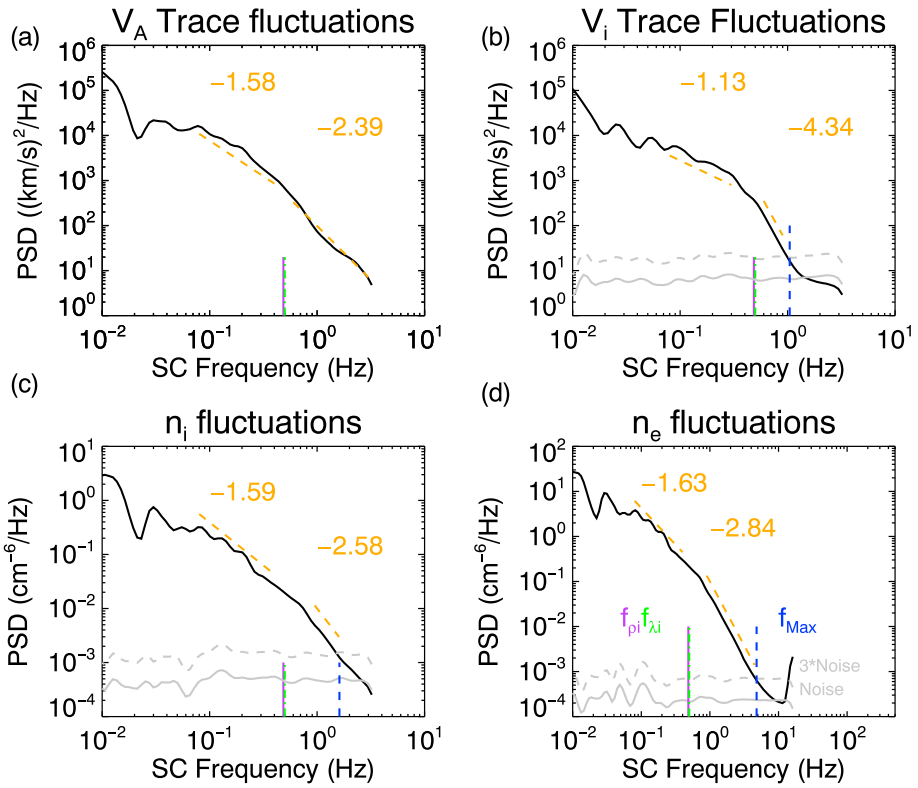

Figure 2. Wavelet power spectral density (PSD) as a function of spacecraft (SC) frame frequency derived from the measurements illustrated in Figure 1 of the trace Alfvén speed fluctuations (a), the trace ion velocity fluctuations (b), the ion density fluctuations (c), and the electron density fluctuations (d). The solid gray curves denote the estimate of the noise floor, the gray dashed curves denote 3 times the noise level, and the blue vertical dashed line denotes the largest physical frequency where the signal-to-noise ratio is equal to 3. Orange dashed lines show the spectral indices of inertial and kinetic ranges fitted for the frequency range that they span. The Taylor shifted ion inertial and gyroradius lengths are denoted by the green dot-dashed and purple solid lines, respectively, but lie on one another as $\beta \sim 1$.

the spacecraft frame (bottom x axis) and of the wavenumber which is derived from the application of Taylor's hypothesis (top x axis). We expect this to be a good approximation as we will detail later.

The orange and dark blue solid curves denote the predictions from two-fluid MHD for the KAW and the KSW, respectively, as derived from Zhao et al. (2014). The simplified low β approximations of the Alfv\'en ratio for KAW and KSW are denoted by dashed lines and are given in equations (3) and (4), respectively.

$$R_{A,\mathrm{KAW}} = \frac{1+\beta\frac{\rho_i^2 k_\perp^2}{1+\rho_i^2 k_\perp^2}}{1+\rho_i^2 k_\perp^2+\beta\frac{\rho_i^2 k_\perp^2}{1+\rho_i^2 k_\perp^2}}. \tag{3}$$

$$R_{A,\mathrm{KSW}} = \frac{1+2\rho_i^2 k_\perp^2}{\beta}. \tag{4}$$

More details can be found in Appendix A. It is important to note that these equations assume a low plasma β but approximate the more complex solutions well especially for the KAW case.

In the above equations, we use the mean value of β obtained from measurements and the wavenumber from Taylor's hypothesis, and we also assume that there is a strong anisotropy in wavevectors ($k_\perp \gg k_\parallel$), which is measured to be the case in the magnetosheath (e.g., Chen & Boldyrev, 2017; Gershman et al., 2018; Narita & Glassmeier, 2005).

A χ^2 test is performed for both KAW and KSW curves for the full two-fluid expressions (subscript TF) and the simplified low β expressions (subscript LB) between spacecraft frame frequencies of 0.08 and 1 Hz to avoid the cone of influence present at large scales when using a wavelet transform at low frequencies (Torrence &

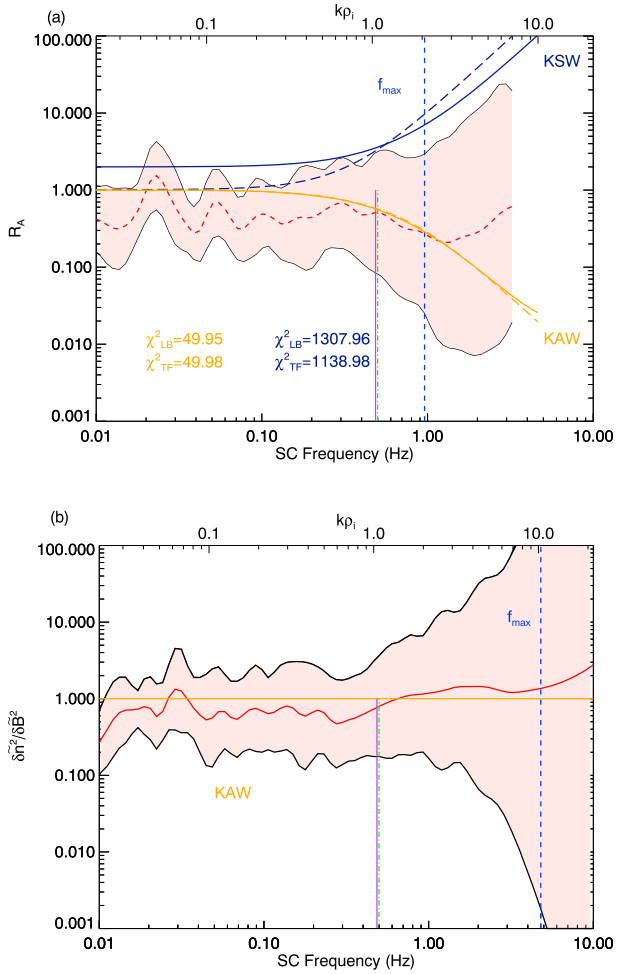

Figure 3. (a) The Alfvén ratio defined by equation (2) as a function of the frequency observed in the spacecraft frame. The red dashed line represents R_A as derived from the observations illustrated in Figure 1. The orange dashed line represents the predicted $R_{A,KAW}$ as obtained from equation (3), whereas the dark blue dashed line represents the predicted $R_{A,KSW}$ as obtained from equation (4) where the low *beta* approximation is used; χ^2 values are denoted by the subscript LB. The solid orange and dark blue lines represent the curves from the full two-fluid equations, and χ^2 are denoted by subscript TF. (b) The solid red line represents the dimensionless ratio of the square of the normalized electron density fluctuations defined in equation (5) divided by the normalized magnetic field fluctuation energy density defined in equation (6) as a function of the frequency observed in the spacecraft frame as derived from the observations illustrated in Figure 1. In both panels, the rose-colored area denotes the 1σ relative error as described in the text. In both panels, the green dot-dashed and purple solid lines denote the Taylor shifted inertial length and gyroradius, respectively, and the blue vertical dashed line f_{max} denotes the maximum physical frequency. KAW = kinetic Alfvén wave; KSW = kinetic slow wave.

Compo, 1998) and the influence of noise at high frequencies. In the considered range, it is clear from Figure 3a that the KAW prediction for the Alfvén ratio is a better fit to the observations than the KSW prediction.

Figure 3b shows the normalized ratio of electron density $\tilde{n_e}$ and magnetic field fluctuations $\tilde{\mathbf{B}}$, defined as

$$\tilde{n_e} = \left(1 + \frac{T_i}{T_e}\right)^{1/2} \frac{v_s}{v_A} \left[1 + \left(\frac{v_s}{v_A}\right)^2 \left(1 + \frac{T_i}{T_e}\right)\right]^{1/2} \frac{n_e}{n_0}, \tag{5}$$

$$\tilde{\mathbf{B}} = \frac{\mathbf{B}}{|\mathbf{B}|}. \tag{6}$$

where v_s is the sound speed (Boldyrev et al., 2013; Chen & Boldyrev, 2017; Chen, Boldyrev, et al., 2013; O. W. Roberts, Narita, Li, et al., 2017).

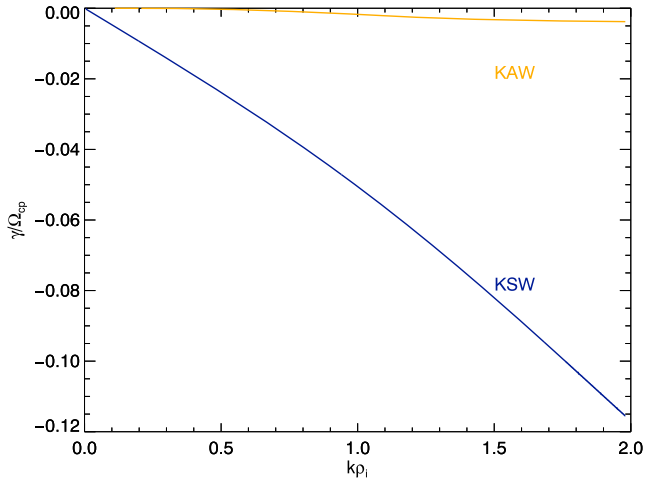

Figure 4. Predicted kinetic damping rates for the KAW (orange) and KSW (blue) calculated assuming a Maxwellian distribution for a wave propagation angle of 88° from the mean magnetic field direction and for plasma $\beta = 0.98$ and $T_e/T_i = 0.084$. KAW = kinetic Alfvén wave; KSW = kinetic slow wave.

For this normalization, it is expected that magnetosonic-like fluctuations would have $\delta\tilde{n}_e^2/\delta\tilde{\mathbf{B}}^2 \gg 1$ and KAW-like fluctuations to have $\delta\tilde{n}_e^2/\delta\tilde{\mathbf{B}}^2 \sim 1$ (Boldyrev et al., 2013;Chen, Boldyrev, et al., 2013). At all scales below f_{max}, the ratio is close to 1 suggesting that KAWs are dominant over any magnetosonic fluctuations. Above f_{max}, this ratio increases due to the density measurement reaching the noise floor and its spectrum flattening, while the magnetic spectrum continues to decrease. By ruling out magnetosonic turbulence as the dominant process, it suggests that the fluctuations are KAW- or KSW-like, both of which have low phase speeds for quasi-perpendicular propagation ($v_{ph} < v_A$). This indicates that the application of Taylor's hypothesis at these scales is likely to be valid even when the Alfvén and bulk speeds are comparable (Klein et al., 2014). Furthermore, as argued by Chen and Boldyrev (2017) and Klein et al. (2014), should the hypothesis be broken, the resulting spectra would be shallower; the spectra here are consistent with those which are often seen in the solar wind where $V_i \gg v_A$.

4. Discussion/Summary

To summarize, in the present letter, we have estimated the Alfvén ratio and the normalized ratio of density to magnetic fluctuations in the turbulent magnetosheath by using high-resolution data from the MMS mission. The observed ratios decrease with increasing wavenumber, which is consistent with the predicted values from two-fluid theory (Zhao et al., 2014), as well as linear Vlasov theory (Gary, 1986) for KAW-like fluctuations, as was recently described by Chen and Boldyrev (2017) and Gershman et al. (2018). This complements the results from linear Vlasov theory that KSWs in a plasma where $\beta = 1$ and $T_e < T_i$ are strongly damped (e.g., Gary, 1993). The linear damping rates of both KAWs and KSWs are shown in Figure 4. These calculations are based on a Maxwellian plasma which is known empirically to give similar dispersion relations for other distribution functions; however, the damping rates are very sensitive to the shape of the distribution. Future work will involve investigating the variation of the damping rates for different shapes of the distribution functions. The magnitude of the damping rate is much larger for the KSW suggesting that in the magnetosheath, the KSW cannot exist for more than a few wave cycles in the plasma at $k\rho_i = 1$, whereas the KAW is only lightly damped and can persist to smaller scales.

However, for solar wind, where electrons can be hotter than ions, such as is typical in slow solar wind (e.g., Bruno & Carbone, 2013; Mangeney et al., 1999) and when the plasma $\beta < 1$, it is possible that the KSW can exist and might be an important heating mechanism. In light of the upcoming Parker Solar Probe and Solar Orbiter missions, the Alfvén ratio may be a useful measure for characterizing plasma fluctuations.

The ratio of normalized density and magnetic fluctuations further supports this interpretation and rules out the dominance of magnetosonic-like fluctuations at these scales, at least for the considered interval. In this work, we sought to understand the evolution of the Alfvén ratio with scales and compare to wave models. However, it should be noted that nonlinear intermittent structures may have an influence on the Alfvén ratio

reducing below unity (e.g., Borovsky, 2008). It is important to note that coherent structures can also produce properties such as nonzero magnetic helicity which are commonly interpreted in the wave paradigm. While this is outside the scope of this paper, this will be an interesting avenue to pursue in future, where the multiple spacecraft of MMS and wavelet techniques (Perrone et al., 2016, 2017) will prove useful to identify structures and understand their influence on the Alfvén ratio.

Appendix A: Alfvén Ratio Equation Derivation for Kinetic Alfvén Wave

The Alfvén ratio is defined as

$$R_A = \mu_0 n m_i \frac{|\delta \mathbf{V}_i|^2}{|\delta \mathbf{B}|^2}. \tag{A1}$$

The velocity and magnetic field fluctuations for a kinetic Alfvén wave are defined as (listed as equation C2 in Zhao et al., 2014).

$$\frac{\delta \mathbf{v}_i}{v_A} = -i\lambda_i k_\parallel \frac{\delta B_y}{B_0}\mathbf{e}_x - \frac{\mathcal{L}'^{1/2}}{\mathcal{R}^{1/2}}\frac{\delta B_y}{B_0}\mathbf{e}_y - i\frac{\left(\mathcal{R}-\mathcal{L}+\rho_i^2 k_\perp^2 \lambda_i^2 k_\parallel^2\right)}{\lambda_i k_\perp \mathcal{R}}\frac{\delta B_y}{B_0}\mathbf{e}_z, \tag{A2}$$

$$\delta \mathbf{B} = -i\frac{k_\parallel}{k_\perp}\frac{\left(\mathcal{L}\rho_i^2 k_\perp^2 - \lambda_i^2 k_\parallel^2\right)}{\lambda_i k_\perp \mathcal{R}^{1/2}\mathcal{L}'^{1/2}}\delta B_y \mathbf{e}_x + \delta B_y \mathbf{e}_y + i\frac{\mathcal{L}\rho_i^2 k_\perp^2 - \lambda_i^2 k_\parallel^2}{\lambda_i k_\perp \mathcal{R}^{1/2}\mathcal{L}'^{1/2}}\delta B_y \mathbf{e}_z, \tag{A3}$$

where

$$\mathcal{R} = 1 + \rho_i^2 k_\perp^2, \quad \mathcal{L} = 1 + \lambda_e^2 k_\perp^2, \quad \mathcal{L}' = 1 + \lambda_e^2 k_\perp^2 + \lambda_i^2 k_\parallel^2. \tag{A4}$$

If we substitute equations (A2) and (A3) into equation (A1), we obtain the expression for the Alfvén ratio:

$$R_{A,\mathrm{KAW}} = \frac{\lambda_i^2 k_\parallel^2 + \frac{\mathcal{L}'}{\mathcal{R}} + \frac{\left(\mathcal{R}-\mathcal{L}+\rho_i^2 k_\perp^2 \lambda_i^2 k_\parallel^2\right)^2}{\lambda_i^2 k_\perp^2 \mathcal{R}^2}}{\frac{k_\parallel^2}{k_\perp^2}\frac{\left(\mathcal{L}\rho_i^2 k_\perp^2 - \lambda_i^2 k_\parallel^2\right)^2}{\lambda_i^2 k_\perp^2 \mathcal{R}\mathcal{L}'} + 1 + \frac{\left(\mathcal{L}\rho_i^2 k_\perp^2 - \lambda_i^2 k_\parallel^2\right)^2}{\lambda_i^2 k_\perp^2 \mathcal{R}\mathcal{L}'}}. \tag{A5}$$

Then, assuming a strong anisotropy in the wavevectors ($k_\perp \gg k_\parallel$), we obtain

$$R_{A,\mathrm{KAW}} \simeq \frac{\lambda_i^2 k_\parallel^2 + \frac{\mathcal{L}'}{\mathcal{R}} + \frac{\left(\mathcal{R}-\mathcal{L}+\rho_i^2 k_\perp^2 \lambda_i^2 k_\parallel^2\right)^2}{\lambda_i^2 k_\perp^2 \mathcal{R}^2}}{1 + \frac{\left(\mathcal{L}\rho_i^2 k_\perp^2 - \lambda_i^2 k_\parallel^2\right)^2}{\lambda_i^2 k_\perp^2 \mathcal{R}\mathcal{L}'}}. \tag{A6}$$

Substituting equation (A4) in equation (A6) and ignoring electron inertia $\lambda_e^2 k_\perp^2$ as we are in the limit $\beta \gg m_e/m_i$

$$R_{A,\mathrm{KAW}} \simeq \frac{\frac{1+\lambda_i^2}{k}{}^2{}_\parallel}{1 + \rho_i^2 k_\perp^2 + \lambda_i^2 k_\parallel^2 + \beta\rho_i^2 k_\perp^2 \frac{\left(1+\lambda_i^2 k_\parallel^2\right)^2}{\left(1+\rho_i^2 k_\perp^2\right)^2}} 1 + \frac{\left(\rho_i^2 k_\perp^2 - \lambda_i^2 k_\parallel^2\right)^2}{\lambda_i^2 k_\perp^2 \left(1+\rho_i^2 k_\perp^2\right)\left(1+\lambda_i^2 k_\parallel^2\right)}. \tag{A7}$$

In the low-frequency limit $\omega \ll \omega_{ci}$, $\lambda_i k_\parallel \ll 1$, we finally obtain the expression for the Alfvén ratio for kinetic Alfvén waves used in Figure 3.

$$R_{A,\mathrm{KAW}} \simeq \frac{1 + \beta\frac{\rho_i^2 k_\perp^2}{1+\rho_i^2 k_\perp^2}}{1 + \rho_i^2 k_\perp^2 + \beta\frac{\rho^2 k_\perp^2}{1+\rho_i^2 k_\perp^2}}. \tag{A8}$$

Acknowledgments
We thank all the people involved in the MMS project for the high-quality data provided. O. R. and S. T. R. are funded by an ESA Science Research Fellowship and acknowledge several helpful discussions of the joint ESTEC/ESAC heliophysics group. S. T. R. also acknowledges support from the ISSI's international team *MMS and CLUSTER observations of magnetic reconnection* and from the science faculty of the European Space Astronomy Centre (ESAC). The data used in this work are available to the public in the MMS Science Data Center (https://lasp.colorado.edu/mms/sdc/public/).

References

Alexandrova, O., Chen, C. H. K., Sorriso-Valvo, L., Horbury, T. S., & Bale, S. D. (2013). Solar wind turbulence and the role of ion instabilities. *Space Science Reviews*, *178*, 25–63. https://doi.org/10.1007/978-1-4899-7413-6_3

Alexandrova, O., Lacombe, C., & Mangeney, A. (2008). Solar wind vs magnetosheath turbulence and Alfvén vortices. *Nonlinear Processes in Geophysics*, *215*, 95108. https://doi.org/10.5194/npg-15-95-2008

Alexandrova, O., Lacombe, C., Mangeney, A., Grappin, R., & Maksimovic, M. (2012). Solar wind turbulent spectrum at plasma kinetic scales. *Astrophysics Journal*, *760*(2), 121. https://doi.org/10.1088/0004-637X/760/2/121

Alexandrova, O., Mangeney, A., Maksimovic, M., Lacombe, C., Cornilleau-Wehrlin, N., Lucek, E. A., et al. (2004). Cluster observations of finite amplitude Alfvén waves and small-scale magnetic filaments downstream of a quasi-perpendicular shock. *Journal of Geophysical Research: Space Physics*, *109*, A05207. https://doi.org/10.1029/2003JA010056

Alexandrova, O., Saur, J., Lacombe, C., Mangeney, A., Schwartz, S. J., Mitchell, J., et al. (2010). Solar wind turbulent spectrum from MHD to electron scales. In *AIP Conf. Proc.*, *1216*, (pp. 144–147). Saint-Malo, France https://doi.org/10.1063/1.3395821

Bale, S., Kellogg, P. J., Mozer, F. S., Horbury, T. S., & Reme, H. (2005). Measurement of the electric fluctuation spectrum of magnetohydrodynamic turbulence. *Physical Review Letters*, *94*, 215002. https://doi.org/10.1103/PhysRevLett.94.215002

Barnes, A. (1966). Collisionless damping of hydromagnetic waves. *Physics of Fluids*, *9*(8), 1483. https://doi.org/10.1063/1.1761882

Boldyrev, S., Horaites, K., Xia, Q., & Perez, J. C. (2013). Toward a theory of astrophysical plasma turbulence at subproton scales. *Astrophysical Journal*, *777*(1), 16. https://doi.org/10.1088/0004-637X/777/1/41

Borovsky, J. E. (2008). Flux tube texture of the solar wind: Strands of the magnetic carpet at 1 AU? *Journal of Geophysical Research: Space Physics*, *113*, A08110. https://doi.org/10.1029/2007JA012684

Bruno, R., Bavassano, B., & Villante, U. (1985). Evidence for long period Alfvén waves in the inner solar system. *Journal of Geophysical Research: Space Physics*, *90*(A5), 4373. https://doi.org/10.1029/JA090iA05p04373

Bruno, R., & Carbone, V. (2013). The solar wind as a turbulence laboratory. *Living Reviews in Solar Physics*, *10*(2), 1–208. https://doi.org/10.12942/lrsp-2013-2

Bruno, R., D'Amicis, R., Bavassano, B., Carbone, V., & Sorriso-Valvo, L. (2007). Magnetically dominated structures as an important component of the solar wind turbulence. *Annales de Geophysique*, *25*, 1913–1927. https://doi.org/10.5194/angeo-25-1913-2007

Bruno, R., Trenchi, L., & Telloni, D. (2014). Spectral slope variation at proton scales from fast to slow solar wind. *Astrophysical Journal Letters*, *793*, L15. https://doi.org/10.1088/2041-8205/793/1/L15

Burch, J. L., Moore, T. E., Torbert, R. B., & Giles, B. L. (2016). Magnetospheric multiscale overview and science objectives. *Space Science Review*, *199*, 5–21. https://doi.org/10.1007/s11214-015-0164-9

Celnikier, L. M., Harvey, C. C., Jegou, R., Kemp, M., & Moricet, P. (1983). A determination of the electron density fluctuation spectrum in the solar wind, using the ISEE propagation experiment. *Astronomy and Astrophysics*, *126*, 293–298.

Chandran, B. D. G., Quataert, E., Howes, G. G., Xia, Q., & Pongkitiwanichakul, P. (2009). Constraining low-frequency Alfvénic turbulence in the solar wind using density-fluctuation measurements. *Astrophysical Journal*, *707*, 1668–1675. https://doi.org/10.1088/0004-637X/707/2/1668

Chen, C. H. K., Bale, S. D., Salem, C. S., & Maruca, B. A. (2013). Residual energy spectrum of solar wind turbulence. *The Astrophysical Journal*, *125*, 1–10. https://doi.org/10.1088/0004-637X/770/2/125

Chen, C. H. K., & Boldyrev, S. (2017). Nature of kinetic scale turbulence in the Earth's magnetosheath, *842*(2), 122. https://doi.org/10.3847/1538-4357/aa74e0

Chen, C. H. K., Boldyrev, S., Xia, Q., & Perez, J. C. (2013). Nature of subproton scale turbulence in the solar wind. *Physical Review Letters*, *225002*(May), 1–5. https://doi.org/10.1103/PhysRevLett.110.225002

Chen, C., Howes, G. G., Bonnell, J. W., Mozer, F. S., Klein, K. G., & Bale, S. (2012). Kinetic scale density fluctuations in the solar wind. In *SOLAR WIND 13: Proceeding of the Thirteenth International Solar Wind Conference Solar Wind*, *1539* (pp. 143–146). Pasadena, CA https://doi.org/10.1063/1.4811008

Chen, C. H. K., Salem, C. S., Bonnell, J. W., Mozer, F. S., & Bale, S. D. (2012). Density fluctuation spectrum of solar wind turbulence between ion and electron scales. *Physical Reviews Letters*, *109*, 035001. https://doi.org/10.1103/PhysRevLett.110.225002

Gary, S. P. (1993). *Theory of space plasma microinstabilities*. Cambridge: Cambridge University Press.

Gary, S. P. (1986). Low-frequency waves in a high-beta collisionless plasma: Polarization, compressibility and helicity. *Physics of Plasmas*, *25*, 022303. https://doi.org/10.1017/S0022377800011442 J. Plasma Physics (1986), vol. 35, part 3, pp. 431–447.

Génot, V., Budnik, E., Hellinger, P., Passot, T., Belmont, G., Trávníček, P. M., et al. (2009). Mirror structures above and below the linear instability threshold: Cluster observations, fluid model and hybrid simulations. *Annals of Geophysics*, *27*(2), 601–615. https://doi.org/10.5194/angeo-27-601-2009

Gershman, D., Viñas, A., Dorelli, J. C., Goldstein, M. L., Shuster, J., Avanov, L. A., et al. (2018). Energy partitioning constraints at kinetic scales in low-β turbulence. *Physics of Plasmas*, *25*, 022303. https://doi.org/10.1063/1.5009158

He, J., Tu, C.-Y., Marsch, E., & Yao, S. (2012). Do oblique Alfvén/ion-cyclotron or fast-mode/whistler waves dominate the dissipation of solar wind turbulence near the proton inertial length? *Astrophysical Journal Letters*, *745*(1), L8. https://doi.org/10.1088/2041-8205/745/1/L8

Hellinger, P., Travnicek, P., Kasper, J. C., & Lazarus, A. J. (2006). Solar wind proton temperature anisotropy: Linear theory and WIND/SWE observations. *Geophysical Research Letters*, *33*, L09101. https://doi.org/10.1029/2006GL025925

Howes, G. G. (2013). Alfven wave collisions, the fundamental building block of plasma turbulence. I. Asymptotic solution. *Physics of Plasmas*, *20*, 11. https://doi.org/10.1063/1.4812805

Howes, G. G., Bale, S. D., Klein, K. G., Chen, C. H. K., Salem, C. S., & TenBarge, J. M. (2012). The slow-mode nature of compressible wave power in solar wind turbulence. *The Astrophysical Journal*, *753*, L19. https://doi.org/10.1088/2041-8205/753/1/L19

Howes, G. G., TenBarge, J. M., Dorland, W., Quataert, E., Schekochihin, A. A., Numata, R., & Tatsuno, T. (2011). Gyrokinetic simulations of solar wind turbulence from ion to electron scales. *Physical Reviews Letters*, *035004*, 107. https://doi.org/10.1103/PhysRevLett.107.035004

Kiyani, K. H., Chapman, S. C., Sahraoui, F., Hnat, B., Fauvarqu, O., & Khotyanitsev, Y. (2013). Enhanced magnetic compressibility and isotropic scale invariance at sub-ion Larmor scales in solar wind turbulence. *The Astrophysical Journal*, *763*, 10. https://doi.org/10.1088/0004-637X/763/1/10

Kiyani, K. H., Osman, K. T., & Chapman, S. C. (2015). Dissipation and heating in solarwind turbulence: fromthe macro to themicro and back again. *Philosophical Transactions of the Royal Society A: Mathematical, Physical and Engineering Sciences*, *373*(2041), 20140155. ISSN 1364-503×. https://doi.org/10.1098/rsta.2014.0155

Klein, K. G., Howes, G. G., TenBarge, J. M., & Podesta, J. J. (2014). Physical interpretation of the angle-dependent magnetic helicity spectrum in the solar wind: The nature of turbulent fluctuations near the proton gyroradius scale. *The Astrophysical Journal*, *785*(138), 26.

Lacombe, C., Alexandrova, O., Matteini, L., & The Astrophysical Journal (2017). Anisotropies of the magnetic field fluctuations at kinetic scales in the solar wind: Cluster observations, *848*, 45. https://doi.org/10.3847/1538-4357/aa8c06

Lucek, E. A., Constantinescu, D., Goldstein, M. L., Pickett, J., Pinçon, J. L., Sahraoui, F., et al. (2005). The magnetosheath. *Space Science Reviews*, *118*(1-4), 95–152. https://doi.org/10.1007/s11214-005-3825-2

Mangeney, A., Salem, C., Lacombe, J.-L., Bougeret, C., Perche, R., Manning, P. J., et al. (1999). WIND observations of coherent electrostatic waves in the solar wind. *Annals of Geophysics*, *17*, 307–320. https://doi.org/10.1007/s00585-999-0307-y

Matthaeus, W. H., & Goldstein, M. L. (1982). Measurement of the rugged invariants of magnetohydrodynamic turbulence in the solar wind. *Journal of Geophysical Research: Space Physics*, *87*(A8), 6011–6028. https://doi.org/10.1029/JA087iA08p06011
Narita, Y. (2018). Space time structure and wavevector anisotropy in space plasma turbulence. *Living Reviews in Solar Physics*, *15*(1), 2. https://doi.org/10.1007/s41116-017-0010-0
Narita, Y., & Glassmeier, K.-H. (2005). Dispersion analysis of low-frequency waves through the terrestrial bow shock. *Journal of Geophysical Research: Space Physics*, *110*, A12215. https://doi.org/10.1029/2005JA011256
Narita, Y., & Glassmeier, K.-H. (2009). Spatial aliasing and distortion of energy distribution in the wave vector domain under multi-spacecraft measurements. *Annals of Geophysics*, *27*(8), 3031–3042. https://doi.org/10.5194/angeo-27-3031-2009
Narita, Y., & Marsch, E. (2015). Kinetic slow mode in the solar wind and its possible role in turbulence dissipation and ion heating. *The Astrophysical Journal*, *805*(1), 24. https://doi.org/10.1088/0004-637X/805/1/24
Narita, Y., & Motschmann, U. (2017). Ion-scale sideband waves and filament formation: Alfvénic impact on heliospheric plasma turbulence. *Front Phys*, *5*(8), 1–8. https://doi.org/10.3389/fphy.2017.00008
Passot, T., Sulem, P. L., & Tassi E. (2017). Electron-scale reduced fluid models with gyroviscous effects. *Journal of Plasma Physics*, *83*(04), 715830402. https://doi.org/10.1017/S0022377817000514
Perrone, D., Alexandrova, O., Mangeney, A., Maksimovic, M., Lacombe, C., Rakoto, V., et al. (2016). Compressive coherent structures at ion scales in the slow solar wind. *The Astrophysical Journal*, *826*(2), 196. https://doi.org/10.3847/0004-637X/826/2/196
Perrone, D., Alexandrova, O., Roberts, O. W., Lion, S., Lacombe, C., Walsh, A., et al. (2017). Coherent structures at ion scales in fast solar wind: Cluster observations. *The Astrophysical Journal*, *849*(1), 49. https://doi.org/10.3847/1538-4357/aa9022
Perschke, C., Narita, Y., Motschmann, U., & Glassmeier, K.-H. (2014). Multi-spacecraft observations of linear modes and sideband waves in ion-scale solar wind turbulence. *The Astrophysical Journal*, *793*, L25. https://doi.org/10.1088/2041-8205/793/2/L25
Perschke, C., Narita, Y., Motschmann, U., & Glassmeier, K.-H. (2016). Observational test for a random sweeping model in solar wind turbulence. *Physical Reviews Letters*, *116*(125101), 1–5. https://doi.org/10.1103/PhysRevLett.116.125101
Podesta, J. J. (2006). Evidence of kinetic Alfvén waves in the solar wind at 1 AU. *Journal of Geophysical Research*, *111*, A10109. https://doi.org/10.1029/2006JA011834
Podesta, J. J. (2013). Evidence of kinetic Alfvèn waves in the solar wind at 1 AU. *Solar Physics*, *286*(2), 529–548. https://doi.org/10.1007/s11207-013-0258-z
Pollock, C., Moore, T., Jacques, A., Burch, J., Gliese, U., Saito, Y., et al. (2016). Fast plasma investigation for magnetospheric multiscale. *Space Science Reviews*, *199*(1-4), 331–406. https://doi.org/10.1007/s11214-016-0245-4
Roberts, O. W., Alexandrova, O., Kajdič, P., Turc, L., Perrone, D., Escoubet, C. P., & Walsh, A. (2017). Variability of the magnetic field power spectrum in the solar wind at electron scales. *The Astrophysical Journal*, *850*(2), 120. https://doi.org/10.3847/1538-4357/aa93e5
Roberts, D. A., Goldstein, M. L., & Klein, L. W. (1990). The amplitudes of interplanetary fluctuations: Stream structure, heliocentric distance, and frequency dependence. *Journal of Geophysical Research*, *95*(A4), 4203–4216.
Roberts, O. W., Li, X., Alexandrova, O., & Li, B. (2016). Observation of an MHD Alfvén vortex in the slow solar wind. *Journal of Geophysical Research: Space Physics*, *121*, 3870–3881. https://doi.org/10.1002/2015JA022248
Roberts, O. W., Li, X., & Jeska, L. (2015). A statistical study of the solar wind turbulence at ion kinetic scales using the k-filtering technique and cluster data. *The Astrophysical Journal*, *802*(2), 1–13. https://doi.org/10.1088/0004-637X/802/1/2
Roberts, O. W., Li, X., & Li, B. (2013). Kinetic plasma turbulence in the fast solar wind measured by Cluster. *The Astrophysical Journal*, *769*(58), 8. https://doi.org/10.1088/0004-637X/769/1/58
Roberts, O. W., Narita, Y., & Escoubet, C. P. (2017). Direct measurement of anisotropic and asymmetric wave vector spectrum in ion-scale solar wind turbulence. *The Astrophysical Journal*, *851*(1), L11. https://doi.org/10.3847/2041-8213/aa9bf3
Roberts, O. W., Narita, Y., & Escoubet, C. P. (2018a). Multi-scale analysis of compressible fluctuations in the solar wind. *Annals of Geophysics*, *36*, 4752. https://doi.org/10.5194/angeo-36-47-2018
Roberts, O. W., Narita, Y., & Escoubet, C. P. (2018b). Three dimensional density and compressible magnetic structure in solar wind turbulence. *Annals of Geophysics*, *36*, 527–539. https://doi.org/10.5194/angeo-36-527-2018
Roberts, O. W., Narita, Y., Li, X., Escoubet, C. P., & Laakso, H. (2017). Multipoint analysis of compressive fluctuations in the fast and slow solar wind. *Journal of Geophysical Research: Space Physics*, *122*, 6940–6963. https://doi.org/10.1002/2016JA023552
Russell, C. T., Anderson, B. J., Baumjohann, W., Bromund, K. R., Dearborn, D., Fischer, D., et al. (2016). The magnetospheric multiscale magnetometers. *Space Science Reviews*, *199*(1-4), 189–256. https://doi.org/10.1007/s11214-014-0057-3
Šafránková, J., Nemecek, Z., Nemec, F., Prech, L., Chen, C. H. K., & Zastenker, G. N. (2016). Power spectral density of fluctuations of bulk and thermal speeds in the solar wind. *The Astrophysical Journal*, *825*(2), 121. https://doi.org/10.3847/0004-637X/825/2/121
Šafránková, J., Nemecek, Z., Prech, L., & Zastenker, G. N. (2013). Ion kinetic scale in the solar wind observed. *Physical Review Letters*, *110*(January), 025004. https://doi.org/10.1103/PhysRevLett.110.025004
Sahraoui, F., Goldstein, M. L., Belmont, G., Canu, P., & Rezeau, L. (2010). Three dimensional anisotropic k spectra of turbulence at subproton scales in the solar wind. *Physical Review Letters*, *105*(131101), 1–4. https://doi.org/10.1103/PhysRevLett.105.131101
Salem, C. S., Howes, G. G., Sundkvist, D., Bale, S. D., Chaston, C. C., Chen, C. H. K., & Mozer, F. S. (2012). Identification of kinetic Alfvén wave turbulence in the solar wind. *The Astrophysical Journal*, *745*(1), L9. https://doi.org/10.1088/2041-8205/745/1/L9
Schekochihin, A., Cowley, S. C., Dorland, W., Hammett, G. W., Howes, G., Quataert, E., & Tatsuno, T. (2009). Astrophysical gyrokinetics: Kinetic and fluid turbulent cascades in magnetized weakly collisional plasmas. *The Astrophysical Journal Supplement*, *182*, 310–377. https://doi.org/10.1088/0067-0049/182/1/310
Smith, C. W., Vasquez, B. J., & Hamilton, K. (2006). Interplanetary magnetic fluctuation anisotropy in the inertial range. *Journal of Geophysical Research: Space Physics*, *111*, A09111. https://doi.org/10.1029/2006JA011651
Telloni, D., Bruno, R., & Trenchi, L. (2015). Radial evolution of spectral characteristics of magnetic field fluctuations at proton scales. *The Astrophysical Journal*, *805*, 46. https://doi.org/10.1088/0004-637X/805/1/46
Torrence, C., & Compo, G. P. (1998). A practical guide to wavelet analysis. *Bulletin of the American Meteorological Society*, *79*, 61–78.
Tu, C.-Y., Marsch, E., & Thieme, K. M. (1989). Basic properties of solar wind MHD turbulence near 0. 3 AU analyzed by means of Elsasser variables. *Journal of Geophysical Research*, *94*(89), 11,739–11,759.
Tu, C.-Y., Marsch, E., & Journal of Geophysical Research: Space Physics (2002). Anisotropy regulation and plateau formation through pitch angle diffusion of solar wind protons in resonance with cyclotron waves, *107*(A9), 1249. https://doi.org/10.1029/2001JA000150
Verscharen, D., Chen, C. H. K., & Wicks, R. T. (2017). On kinetic slow modes, fluid slow modes, and pressure-balanced structures in the solar wind. *The Astrophysical Journal*, *840*, 106. https://doi.org/10.3847/1538-4357/aa6a56
Zhao, J. S., Voitenko, Y., Yu, M. Y., Lu, J. Y., & Wu, D. J. (2014). Properties of short-wavelength oblique Alfven and slow waves. *The Astrophysical Journal*, *793*(107), 12. https://doi.org/10.1088/0004-637X/793/2/107